Contents lists available at ScienceDirect

Journal of Advanced Research

Novel topological nodal lines and exotic drum-head-like surface states in synthesized CsCl-type binary alloy TiOs

Xiaotian Wang [a,1], Guangqian Ding [b,1], Zhenxiang Cheng [a,*], Gokhan Surucu [c,d], Xiao-Lin Wang [a,f], Tie Yang [e,*]

[a] Institute for Superconducting and Electronic Materials (ISEM), University of Wollongong, Wollongong 2500, Australia
[b] School of Science, Chongqing University of Posts and Telecommunications, Chongqing 400065, China
[c] Department of Physics, Middle East Technical University, Turkey
[d] Department of Electric and Energy, Ahi Evran University, Turkey
[e] School of Physical Science and Technology, Southwest University, Chongqing 400715, China
[f] ARC centre of Excellence in Future Low Energy Electronics Technologies (FLEET), University of Wollongong, Wollongong, NSW 2500, Australia

GRAPHICAL ABSTRACT
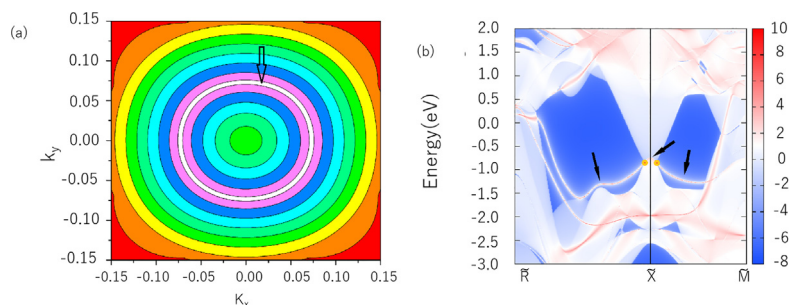
(a) Schematic diagram of TNL (white line) in the $k_z = \pi$ plane of TiOs;
(b) Projected spectrum on the (0 0 1) surface of TiOs

ARTICLE INFO

ABSTRACT

Very recently, searching for new topological nodal line semimetals (TNLSs) and drum-head-like (DHL) surface states has become a hot topic in the field of physical chemistry of materials. Via first principles, in this study, a synthesized CsCl type binary alloy, TiOs, was predicted to be a TNLS with three topological nodal lines (TNLs) centered at the X point in the $k_{x/y/z} = \pi$ plane, and these TNLs, which are protected by mirror, time reversal (T) and spatial inversion (P) symmetries, are perpendicular to one another. The exotic drum-head-like (DHL) surface states can be clearly observed inside and outside the crossing points (CPs) in the bulk system. The CPs, TNLs, and DHL surface states of TiOs are very robust under the influences of uniform strain, electron doping, and hole doping. Spin-orbit coupling (SOC)-induced gaps can be found in this TiOs system when the SOC is taken into consideration. When the SOC is involved, surface Dirac cones can be found in this system, indicating that the topological properties are still maintained. Similar to TiOs, ZrOs and HfOs alloys are TNLSs under the Perdew-Burke-Ernzerhof method. The CPs and the TNLs in both alloys disappear, however, under the Heyd-Scuseria-Ernzerhof method. It is hoped that the DHL surface property in TiOs can be detected by surface sensitive probes in the near future.

* Corresponding authors.
  E-mail addresses: wangxt45@126.com (X. Wang), cheng@uow.edu.au (Z. Cheng), yangtie@swu.edu.cn (T. Yang).
  [1] The contributions of these authors are the same.

Introduction

Over the past 10 years, topological insulators (TIs) [1–5] have received widespread attention from researchers around the world. Due to the band inversion effect [6], the topological insulator has peculiar topological elements, that is, the bulk material exhibits insulating properties, and the surface state exhibits metallic properties. In recent years, investigation of the topological elements has been extended to three-dimensional (3D) semimetal materials [7–11]. This type of material exhibits excellent physical properties [12–14] (Weyl fermion quantum transport and Hall effects) because it contains different types of topological elements. Therefore, following the TIs, topological semimetals (TSMs) can be regarded as a rising star in the field of quantum materials.

To date, three types of TSMs, namely, Dirac semimetals (DSs), Weyl semimetals (WSs), and topological nodal line semimetals (TNLSs), have been predicted in theory. 3D DSs [15–18], including a four-fold degeneracy point near the Fermi level (E_F), can resist external disturbances because they are protected by crystal symmetry and time reversal symmetry (T). Some theoretical works [18–20] have been done, and these efforts have greatly enriched the members of the 3D DS family. It must be mentioned that some novel topological elements predicted by theory have been experimentally confirmed. For example, Neupane et al. [21] systematically studied the electronic structure of Cd_3As_2 by means of high-resolution angular-resolved photoelectron spectroscopy (ARPES), and they stated that the Cd_3As_2 system contains many unusual topological phases. Also, in 3D Na_3Bi, Liu et al [22] detected 3D Dirac fermions by ARPES with linear dispersion along all the momentum directions. If T or reverse symmetry is broken, the 3D DS will evolve into a WS [23]. The well-known WS materials are the TaAs family, and their special topological elements have been experimentally confirmed [24].

For Dirac semimetals and WSs, their crossing points (CPs) are distributed at different k points in the Brillouin zone (BZ), while the CPs near the Fermi level (E_F) of the TNLS will form a closed loop [25–30]. Many different families and different types of TNLSs are theoretically predicted. Normally, the TNLSs can be roughly divided into three categories, i.e., type I TNLS, type II TNLS, and critical type TNLS [27]. A schematic diagram of these three cases is given in Fig. 1c–e. For critical type TNLSs (see Fig. 1b), their distinguishing feature is the presence of energy bands feature an intersection between a horizontal and a dispersive band. In type I TNLSs, these bands (see Fig. 1c) exhibit a traditional conical dispersion in which the electron and hole regions are well separated by energy. In type II TNLSs (see Fig. 1e), these bands are fully tilted, and their electron and hole states coexist at a given energy. Different types of TNLSs have different special properties [29,31], although the different types of TNLSs have a common topological element, namely, the drum-head-like (DHL) surface states [32–34]. Such a two-dimensional (2D) flat surface band state provides another possible way to achieve high temperature superconductivity [35]. Therefore, searching for new, especially synthetic, TNLSs is very necessary. In this work, we will focus on an old synthesized CsCl-type [36] binary alloy, TiOs. The first observation of the ordered CsCl type TiOs system was reported in the work of Laves and Wallbaum [37]. The lattice parameters obtained experimentally by Laves and Wallbaum were $a = b = c = 3.07$ Å. Also, Eremenko [38] observed that TiOs melts congruently at 2160 by differential thermal analysis. The lattice parameters obtained by Eremenko in 1966 were $a/b/c = 3.081$ Å. In this work, by means of first-principles, the lattice parameters of CsCl-type TiOs were optimized, and the calculated results were $a/b/c = 3.806$ Å. The results in this current work are in good agreement with their experimental values mentioned above.

Based on first principles, we predict that TiOs alloy with the CsCl type structure is a TNLS with three type I nodal lines (NLs) that are perpendicular to each other. What is more, interesting DHL surface band states can be observed when the spin–orbit coupling (SOC) effect is absent. The effects of uniform strain and hole-/electron doping on the electronic structures will also be investigated in detail. In addition, the band structures of CsCl type ZrOs and HfOs alloys have been studied using the Perdew-Burke-Ernzerhof (PBE) and Heyd-Scuseria-Ernzerhof (HSE) methods, respectively.

Materials and methods

In this study, the electronic structures of [Ti/Zr/Hf]Os have been calculated using density functional theory (DFT), within the VASP code [39]. The DFT method has proven to be one of the most accurate methods for computation of the electronic structure of solids [40–46]. We also used the projector augmented wave (PAW) method to deal with the interaction between the ion cores and the valence electrons. The PBE [47] parameterization of the generalized gradient approximation (GGA) [48] was selected to describe the exchange and correlation functionals. For the CsCl type [Ti/Zr/Hf]Os systems, a plane-wave basis set cut-off of 500 eV and a Monkhorst-Pack special $15 \times 15 \times 15$ k-point mesh were used in the BZ integration. The unit cell was optimized until the force and total energy were less than 0.005 eV/Å and 0.0000001 eV, respectively. The surface states of TiOs were investigated in this study via the WannierTools software [49], according to the method of maximally localized Wannier functions [50,51].

As an example, the crystal structure of CsCl type TiOs is exhibited in Fig. 1(f), and one can see that the Ti occupies the (0.5,0.5,0.5) site, while the Os occupied the (0,0,0) site. A phonon energy calculation of [Ti/Zr/Hf]Os at their equilibrium lattice constants was performed in NanoAcademic Device Calculator (Nanodcal) code [52]. The results are given in Fig. 2(a–c), and there is no virtual frequency in their phonon band structures, indicating that these compounds in this study are theoretically stable.

Results and discussion

Fig. 1(a) exhibits the selected high symmetry points, i.e., Γ-X-M-Γ-R-X, in the BZ for CsCl type TiOs alloy. Based on these high symmetry points, the band structures of [Ti/Zr/Hf]Os alloys without SOC via the PBE method were calculated, and the results arecollected in Fig. 3(a–c). From them, one can see that there are three CPs near the E_F in total, and they are along Γ-X, X-M, and R-X, respectively. These CPs are composed of two dispersions, and the two dispersion bands form a traditional conical dispersion at the CP, indicating that these CPs are of the first type (see Fig. 1c). What we need to point out is that this Ti/Hf/ZrOs system is protected by T and spatial inversion (P) symmetry, and the spin-less Hamiltonian is always real valued [27], so the observed three CPs in Fig. 3(a)–(c) cannot exist in isolation. Instead, they should belong to a TNL or other types of TN structures. In order to explain this more clearly, in Fig. 4(a) the energy band structure diagram of CsCl-type TiOs in the R-X-M direction is given. From it, one can see two CPs, one along the R-X direction and the other one along the X-M direction, in the $k_z = \pi$ plane. A schematic diagram of the TNL ($k_z = \pi$ plane) where the two CPs are located is also given in Fig. 4(c). Therefore, one can draw the conclusion that an X-centered TNL is formed in the $k_z = \pi$ plane. Due to the cubic symmetry of the material itself, it is easy to see that there are also two equivalent TNLs that can be observed in the $k_x = \pi$ plane and the $k_y = \pi$ plane (see Fig. 5(a)). The TNLs are located in the
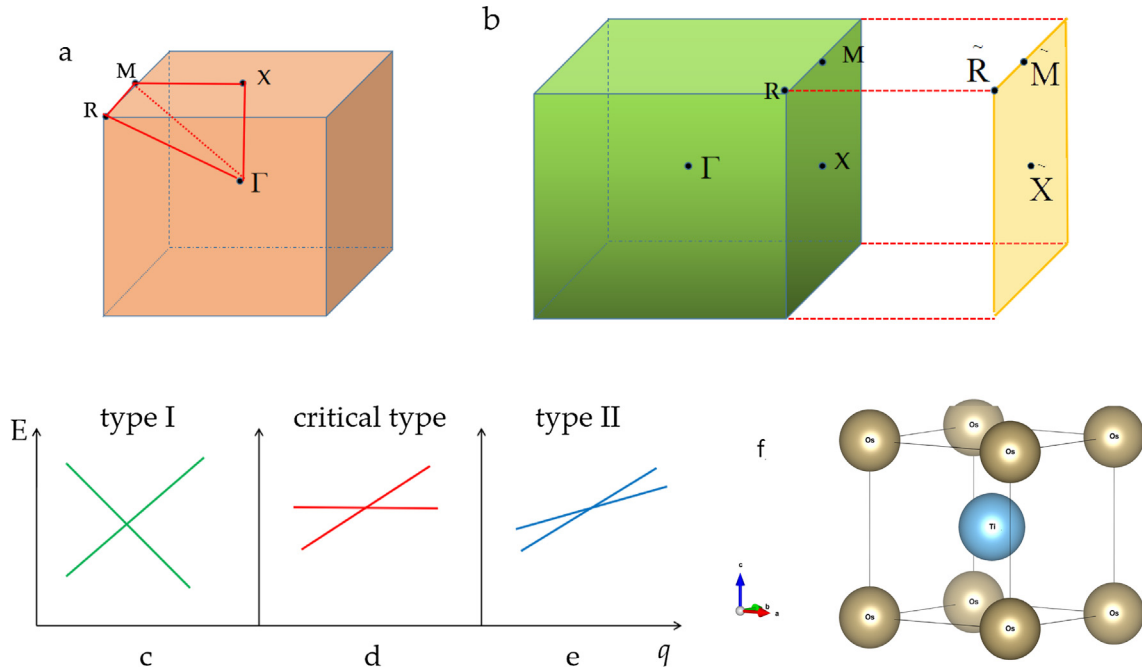
Fig. 1. (a–b) Selected bulk BZ and its projections onto the (0 0 1) surface; (c–e) Three types of crossing points (CPs); (f) crystal structure of CsCl type TiOs.
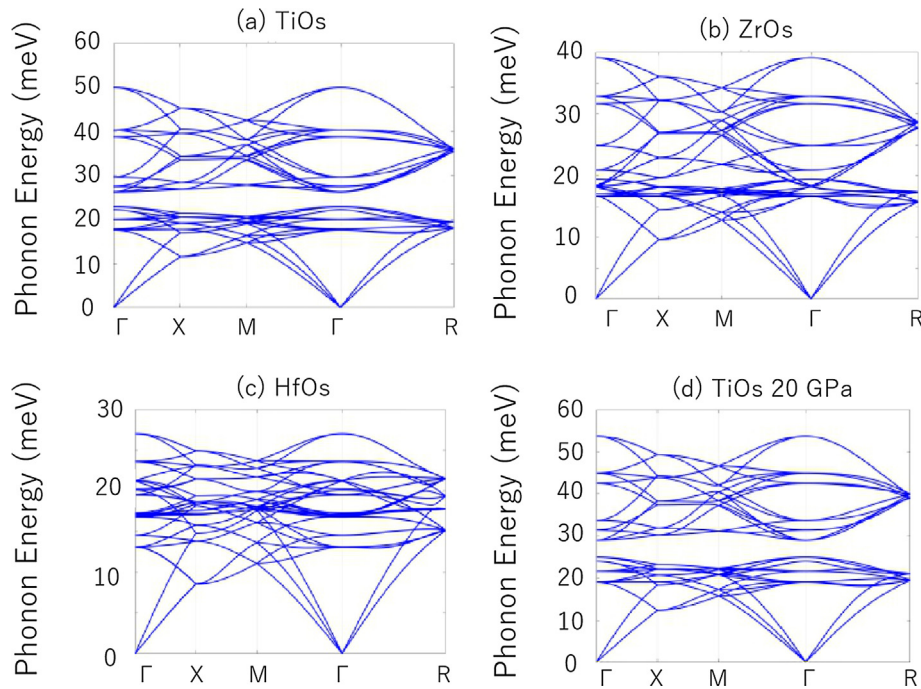

Fig. 2. (a–c) Calculated phonon band structures of [Ti/Zr/Hf]Os, respectively, at 0 GPa; (d) Calculated phonon band structure of TiOs at 20 GPa.

mirror-invariant plane, and these TNLs enjoy the protection of the mirror symmetry M_x, M_y, and M_z, as the three CPs feature opposite M_x, M_y, and M_z eigenvalues.

As shown in Fig. 4(a), one can see that that the CPs along the R-X and X-M paths are type I. To further illustrate that all the CPs along the whole first BZ and the X-centered TNL in the $k_z = \pi$ plane are type I, a more detailed calculation was also performed. For CsCl type TiOs, there are fourfold rotation symmetry and mirror symmetry in the $k_z = \pi$ plane, so we do not need to calculate the energy

band structure for the whole first BZ. Instead, we can use 1/8 part to reflect the nature of the overall BZ, as shown in Fig. 5(b). We divided the 1/8 BZ into 5 parts, so in addition to X-R and X-M, we also selected the four additional directions X-A, X-B, X-C, and X-D. The band structures of TiOs along X-M, X-A, X-B, X-C, X-D, and X-R are given in Fig. 5(c)–(h), respectively. From the figures, one can see that all the CPs along these above-mentioned paths belong to the type I nodal points, and therefore, the TNL in the $k_z = \pi$ plane can also be seen as type I. Noted that a similar
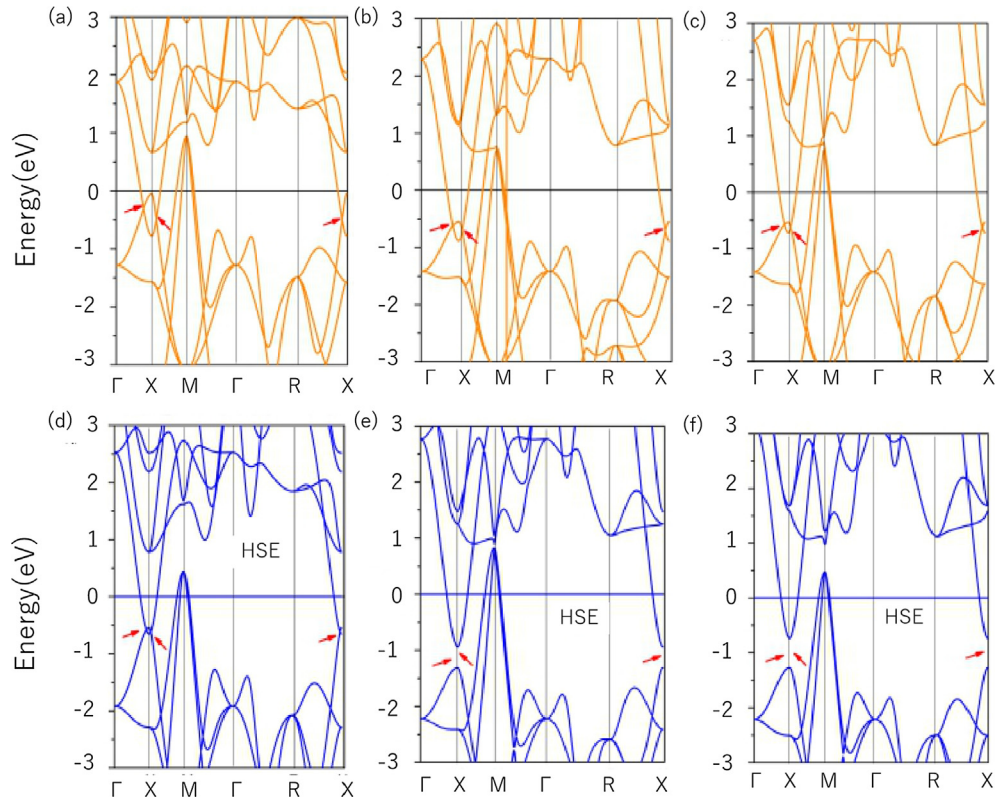
Fig. 3. (a–c) Calculated band structures of [Ti/Zr/Hf]Os, respectively, with the PBE method; (d–f) Calculated band structures of [Ti/Zr/Hf]Os, respectively, with the HSE 06 method.
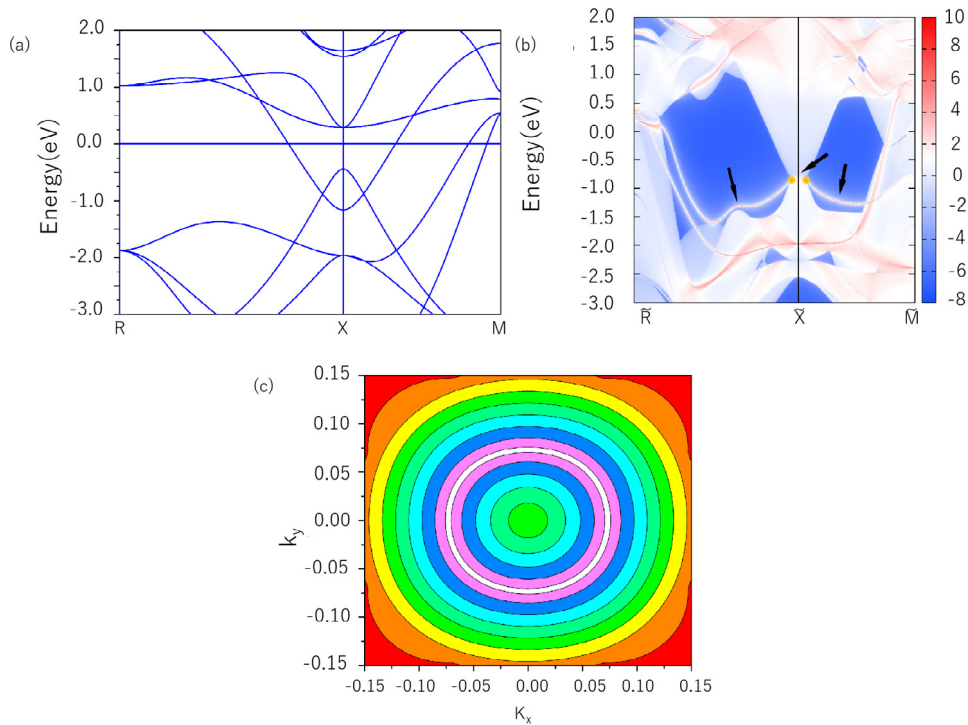

Fig. 4. (a) Calculated band structure of TiOs along the R-X-M direction; (b) Projected spectrum on the (0 0 1) surface of TiOs; (c) Schematic diagram of TNL (white line) in the $k_z = \pi$ plane of TiOs.

situation was reported for CaTe by Du et al. [53] They found that CaTe is a TNLS with three TNLs when the SOC is absent. These three lines are also perpendicular to each other and focused on the M point.

Based on our above discussion, one can conclude that TiOs, ZrOs, and HfOs alloys are newly predicted TNLSs without the SOC effect as calculated by the PBE method. In order to make our results more accurate, the calculations of the band structures of Ti/Zr/HfOs
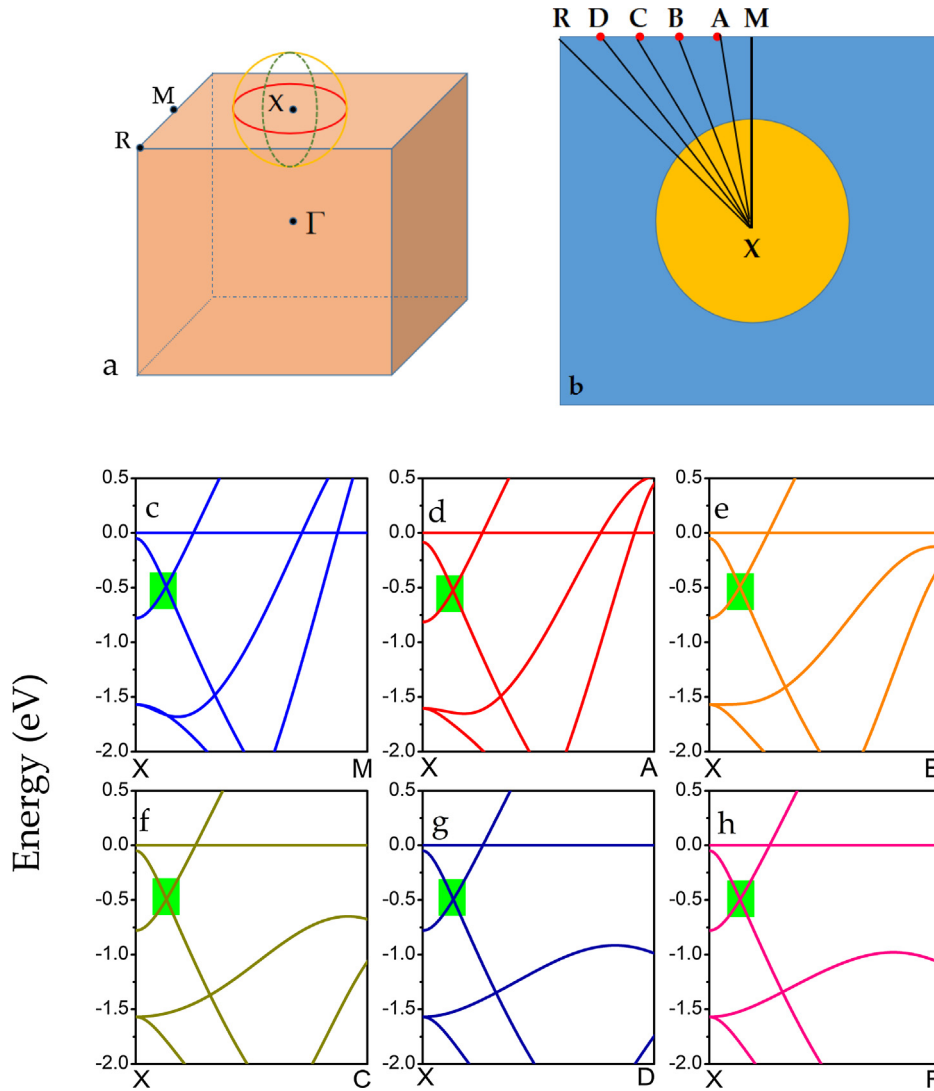
Fig. 5. (a) Schematic diagram of three mutually perpendicular TNLs; (b) selected X-M, X-A, X-B, X-C, X-D, and X-R paths; (c-h) calculated band structures of TiOs with PBE along X-M, X-A, X-B, X-C, X-D, and X-R paths, respectively.

were repeated using the state-of-the-art HSE06 [54] functional, and the results are exhibited in Fig. 3(d)–(f). Unfortunately, for ZrOs and HfOs, the three CPs observed under the PBE method disappeared, and these CPs were converted into three energy gaps. This means that, when using HSE 06, one cannot theoretically observe the novel topological elements of ZrOs and HfOs. For TiOs compound, however, the three CPs still occurred under the HSE 06 method. The DFT+Hubbard correction (DFT+U) calculation for the TiOs system was also carried out in this work, and the results are given in Fig. S1 in the Supporting Information. Therefore, in the following part of this study, we only focus on one material, namely, TiOs, and study its novel physical properties.

The calculated orbital-resolved band structures of TiOs are shown in Fig. 6, where the three CPs are formed by two bands crossing each other, which we have marked as Band 1 and Band 2 (see Fig. 6). Band 1 mainly arises from the Ti-d orbitals, and Band 2 mainly comes from the Os-d orbitals. Therefore, the three CPs are formed by the hybridization between the Ti-d and Os-d orbitals.

In nodal point-type topological materials, their surface states exhibit a Fermi arc type structure. Unlike the topological elements of this class of materials, the surface states of the TNLS should be DHL-type. To confirm the existence of these particular nontrivial

topological, i.e., DHL, surface states, we calculated the projected spectrum of the TiOs (0 0 1) surface along $\tilde{R} - \tilde{X} - \tilde{M}$ in the surface BZ (see Fig. 1(b)), and the obtained results are given in Fig. 4(b). In this Figure, we use two yellow balls to indicate the location of the two band CPs (BCPs) along the R-X-M path, and we use black arrows to highlight the DHL surface states. From the figure, one can clearly see that some DHL surface states are located inside or outside the bulk TNLs. Remarkably, between the two BCPs, the DHL surface state appears to be nearly flat. Based on Kopnin et al.'s work [35], a two-dimensional flat surface state is expected to be a good way to achieve high temperature superconductivity. We hope that the interesting DHL surface states in TiOs can be confirmed by ARPES and scanning tunneling microscopy in the near future.

The effect of uniform strain on the band structure of TiOs was investigated and the results are given in Fig. 7. The optimized lattice constants under different uniform strains can be seen in Table S1. As shown in Fig. 7(a)–(d), 1 GPa, 6 GPa, 10 GPa, and 20 GPa, respectively, were added during the calculations of band structures. In order to verify whether the TiOs is still stable under different uniform strains, the phonon band structures under different strains were calculated. As an example, a phonon band
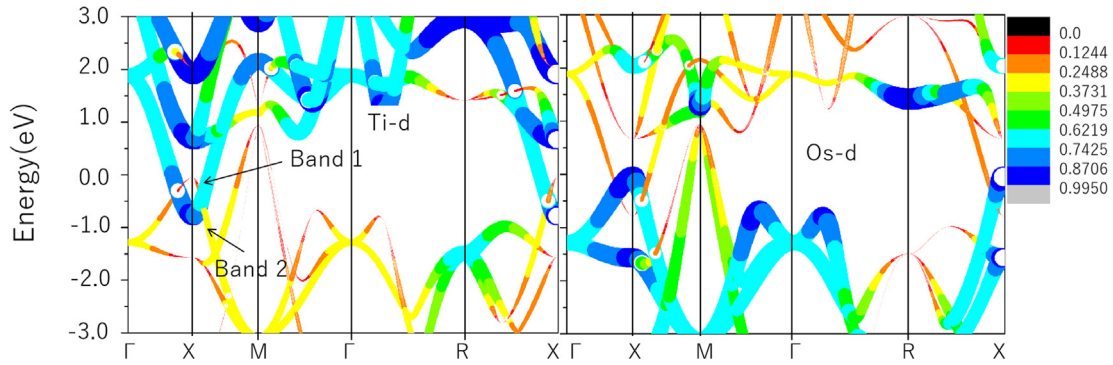
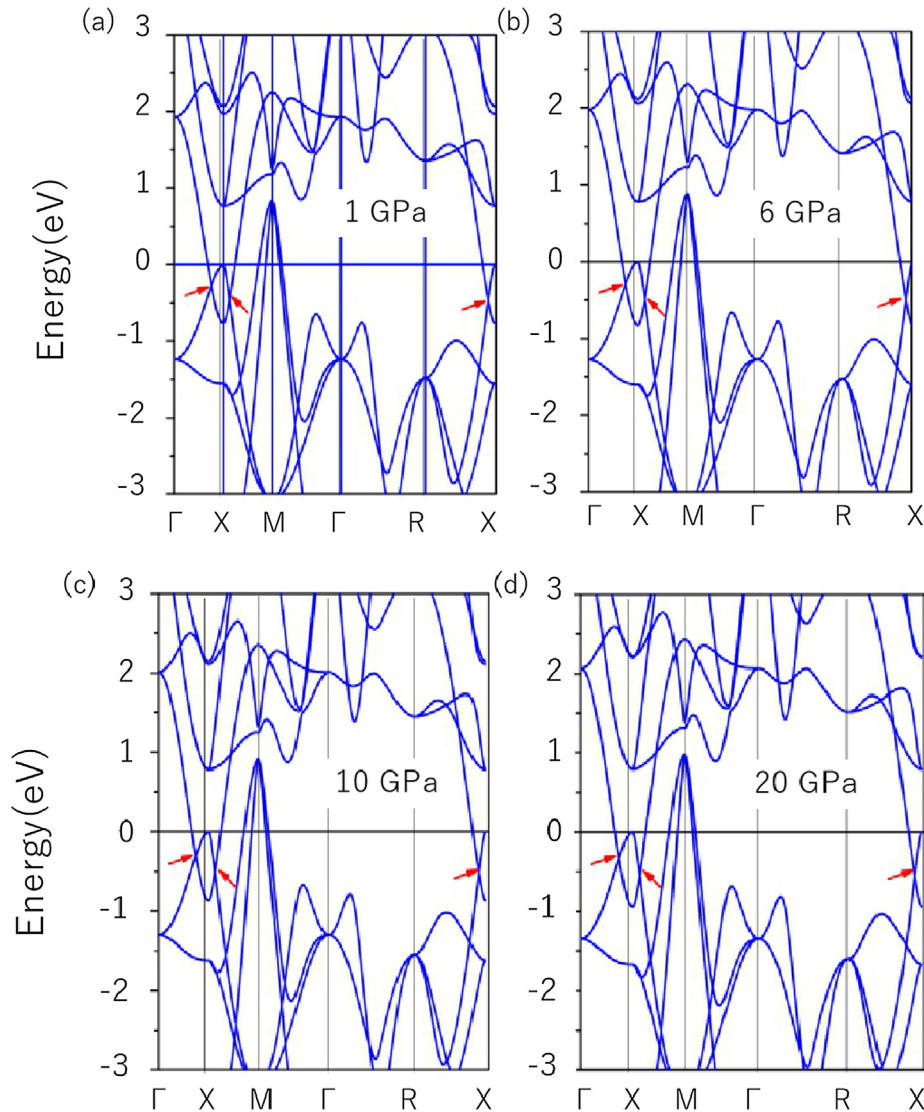**Fig. 6.** Calculated orbital-resolved band structures of TiOs with PBE.

Fig. 7. Band structure of TiOs with PBE under different uniform strains, i.e., 1 GPa (a), 6 GPa (b), 10 GPa (c) and 20 GPa (d), respectively.

structure at 20 GPa is given in Fig. 2(d), and one can see that there is no imaginary frequency present, reflecting the proposition that TiOs under these uniform strains are still stable in terms of theory. From Fig. 7, one can see that the CPs are still maintained, and therefore, the TNL bulk and DHL surface states still exist in CsCl type TiOs under uniform strains ranging from 0 GPa to 20 GPa.

In this work, we will also focus on the effects of electron and hole doping (with a doping concentration of 0.025 carrier per atom [55]) on the band structures of TiOs. The calculated results are given in Fig. 8, where one can see that the shape of the band structure of TiOs did not change except for a slight increase (hole-doping induced) or decrease (electron-doping induced) in the
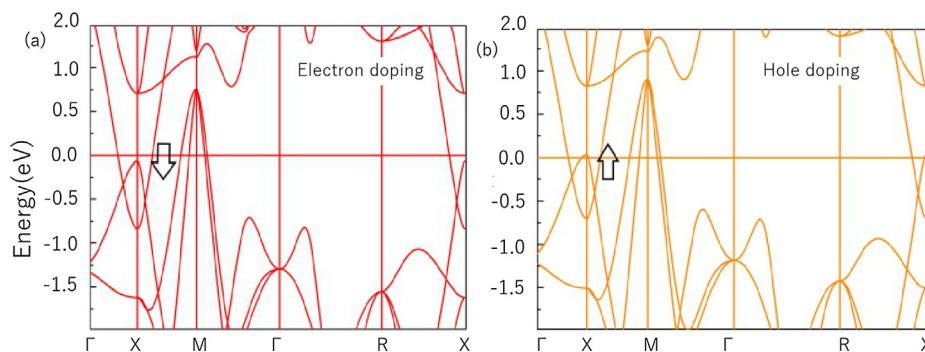
Fig. 8. Band structure of TiOs with PBE under the electron doping effect (a) and the hole doping effect (b), respectively.
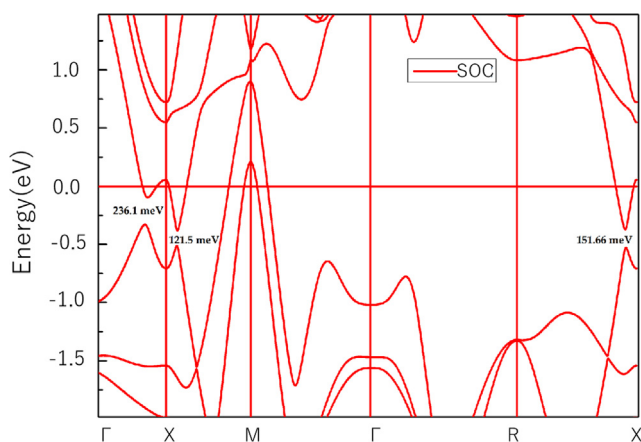

Fig. 9. Band structure of TiOs with PBE and SOC.

Fig. 10. Projected spectrum on the (0 0 1) surface of TiOs with consideration of the SOC effect.

vicinity of the E_F, which indicates that the excellent topological elements, such as the CPs, the TNLs, and the DHL states, in the TiOs system exhibit strong resistance to both the hole doping effect and the electron doping effect. Usually, the Fermi level position, and thereby the carrier concentration, can be adjusted by the use of a gate voltage [56,57].

Before closing, we want to discuss the effects of spin–orbit coupling (SOC) on the TiOs system because this system contains heavy elements. Generally, the SOC effect will drive the TNL states into other different topological phases. To the best of our knowledge, many TNLSs were predicted without considering the effect of the SOC (see Table S2), even though, a transition from the TNL state to an other topological state can be found when the SOC is further added because the SOC generally lifts the degeneracy on the nodal lines. For TiOs, SOC-induced gaps can be found, and the results are exhibited in Fig. 9. Along the X-M and R-X paths, the values of the opened gaps are comparable to that of CaAgAs [58], although the SOC-induced gap along Γ-X is somewhat larger than that of CaAgAs. In order to further confirm that the topological properties still are maintained in TiOs when the SOC effect is involved, the projected spectrum of the TiOs (0 0 1) surface under the influence of SOC is given in Fig. 10. From it, one can observe that the surface Dirac cone has appeared, which confirms the occurrence of the nontrivial topological property even when the SOC effect is considered.

Conclusion

In summary, we have predicted that CsCl-type TiOs, ZrOs, and HfOs compounds are TNLSs in the absence of the SOC effect with the PBE method. Under the HSE06 method, however, only the TNL states and the CPs in TiOs are maintained, and novel DHL surface
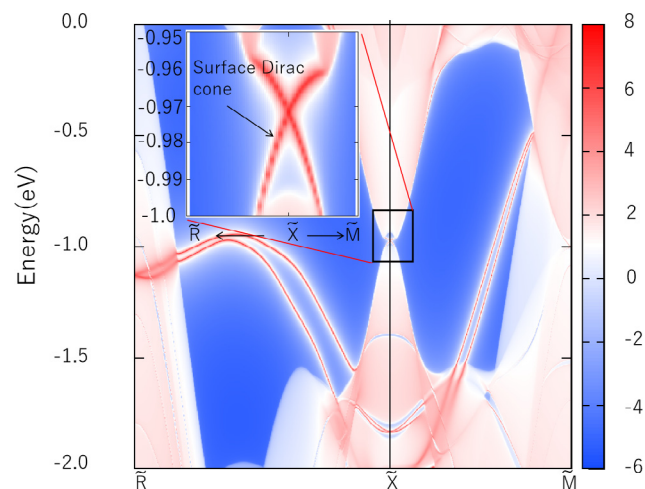
states can be found inside and outside the bulk TNL states of TiOs. With more detailed computations, we can conclude that there are three TNLs centered at the X point and that these TNLs (in the $k_{x/y/z} = \pi$ plane) are perpendicular to one another. These TNLs are protected by the T, P, and mirror symmetries. By calculating the orbital-resolved band structures, one can see that the CPs, and even the TNLs, are formed by the hybridization between the Ti-d and Os-d orbitals. The effects of uniform strain, hole doping and electron doping on the electronic structures were investigated, and the calculated results showed that the TNLs are very robust with respect to the above-mentioned effects. SOC-induced gaps can be found in this system, and the gaps almost comparable with that of CaAgAs compound. Surface Dirac cones can be found in this system when the SOC is taken into consideration, indicating that the topological properties are still maintained. Importantly, TiOs was alloy is easy to synthesize, and its crystal properties have already been well studied experimentally. It is hoped that our current work will bring this old material back to the attention of researchers.

Compliance with ethics requirements

This article does not contain any studies with human or animal subjects.

Declaration of Competing Interest

The authors declare that they have no known competing financial interests or personal relationships that could have appeared to influence the work reported in this paper.

Acknowledgements

Appendix A. Supplementary data

Supplementary data to this article can be found online at https://doi.org/10.1016/j.jare.2019.12.001.

References

[1] Hasan MZ, Kane CL. Colloquium: topological insulators. Rev Mod Phys 2010;82:3045.
[2] Fu L, Kane CL, Mele EJ. Topological insulators in three dimensions. Phys Rev Lett 2007;98:106803.
[3] Moore JE. The birth of topological insulators. Nature 2010;464:194.
[4] Fu L. Topological crystalline insulators. Phys Rev Lett 2011;106:106802.
[5] Qi XL, Zhang SC. Topological insulators and superconductors. Rev Mod Phys 2011;83:1057.
[6] Xiao M, Ma G, Yang Z, Sheng P, Zhang ZQ, Chan CT. Geometric phase and band inversion in periodic acoustic systems. Nature Phys 2015;11:240.
[7] Borisenko S, Gibson Q, Evtushinsky D, Zabolotnyy V, Büchner B, Cava RJ. Experimental realization of a three-dimensional Dirac semimetal. Phys Rev Lett 2014;113:027603.
[8] Yan B, Felser C. Topological materials: Weyl semimetals. Annu Rev Condens Matter Phys 2017;8:337–54.
[9] Wang CM, Lu HZ, Shen SQ. Anomalous phase shift of quantum oscillations in 3D topological semimetals. Phys Rev Lett 2016;117:077201.
[10] Liu ZK, Jiang J, Zhou B, Wang J, Zhang Y, Weng H, et al. A stable three-dimensional topological Dirac semimetal Cd_3As_2. Nature Mater 2014;13:677.
[11] Young SM, Zaheer S, Teo JCY, Kane C, Mele E, Rappe AM. Dirac semimetal in three dimensions. Phys Rev Lett 2012;108:140405.
[12] Hosur P, Qi X. Recent developments in transport phenomena in Weyl semimetals. CR Phys 2013;14:857–70.
[13] Vazifeh MM, Franz M. Electromagnetic response of Weyl semimetals. Phys Rev Lett 2013;111:027201.
[14] Zyuzin AA, Burkov AA. Topological response in Weyl semimetals and the chiral anomaly. Phys Rev B 2012;86:115133.
[15] Armitage NP, Mele EJ, Vishwanath A. Weyl and Dirac semimetals in three-dimensional solids. Rev Mod Phys 2018;90:015001.
[16] Thakur A, Sadhukhan K, Agarwal A. Dynamic current-current susceptibility in three-dimensional Dirac and Weyl semimetals. Phys Rev B 2018;97:035403.
[17] Goyal M, Galletti L, Salmani-Rezaie S, Schumann T, Kealhofer DA, Stemmer S. Thickness dependence of the quantum Hall effect in films of the three-dimensional Dirac semimetal Cd_3As_2. APL Mater 2018;6:026105.
[18] Du Y, Wan B, Wang D, Sheng L, Duan CG, Wan X. Dirac and weyl semimetal in XYBi (X = Ba, Eu; Y = Cu, Ag and Au). Sci Rep 2015;5:14423.
[19] Wang Z, Weng H, Wu Q, Dai X, Fang Z. Three-dimensional Dirac semimetal and quantum transport in Cd_3As_2. Phys Rev B 2013;88:125427.
[20] Wang Z, Sun Y, Chen XQ, Franchini C, Xu G, Weng H, et al. Dirac semimetal and topological phase transitions in A_3Bi (A = Na, K, Rb). Phys Rev B 2012;85:195320.
[21] Neupane M, Xu SY, Sankar R, Alidoust N, Bian G, Liu C, et al. Observation of a three-dimensional topological Dirac semimetal phase in high-mobility Cd_3As_2. Nature Commun 2014;5:3786.
[22] Liu ZK, Zhou B, Zhang Y, Wang Z, Weng H, Prabhakaran D, et al. Discovery of a three-dimensional topological Dirac semimetal, Na_3Bi. Science 2014;343:864–7.
[23] Burkov AA, Balents L. Weyl semimetal in a topological insulator multilayer. Phys Rev Lett 2011;107:127205.
[24] Lv BQ, Weng HM, Fu BB, Wang XP, Miao H, Ma J, et al. Experimental discovery of Weyl semimetal TaAs. Phys Rev X 2015;5:031013.
[25] Zhou N, Zhou P, Li J, Zhong J. Si-Cmma: A silicon thin film with excellent stability and Dirac nodal loop. Phys Rev B 2019;100:115425.
[26] Zhang X, Jin L, Dai X, Liu G. Highly anisotropic type-II nodal line state in pure titanium metal. Appl Phys Lett 2018;112:122403.
[27] Liu G, Jin L, Dai X, Chen G, Zhang X. Topological phase with a critical-type nodal line state in intermetallic CaPd. Phys Rev B 2018;98:075157.
[28] Zhang X, Yu ZM, Lu Y, Sheng XL, Yang HY, Yang S. Hybrid nodal loop metal: Unconventional magnetoresponse and material realization. Phys Rev B 2018;97:125143.
[29] Li S, Yu ZM, Liu Y, Guan S, Wang SS, Zhang X, et al. Type-II nodal loops: Theory and material realization. Phys Rev B 2017;96:081106.
[30] Jin L, Zhang XM, Dai XF, Wang LY, Liu HY, Liu GD. Screening topological materials with a CsCl-type structure in crystallographic databases. IUCrJ 2019;6:688–94.
[31] Hyart T, Heikkilä TT. Momentum-space structure of surface states in a topological semimetal with a nexus point of Dirac lines. Phys Rev B 2016;93:235147.
[32] Burkov AA, Hook MD, Balents L. Topological nodal semimetals. Phys Rev B 2011;84:235126.
[33] Yu R, Weng H, Fang Z, Dai X, Hu X. Topological node-line semimetal and Dirac semimetal state in antiperovskite Cu_3PdN. Phys Rev Lett 2015;115:036807.
[34] Kim Y, Wieder BJ, Kane CL, Rappe AM. Dirac line nodes in inversion-symmetric crystals. Phys Rev Lett 2015;115:036806.
[35] Kopnin NB, Heikkilä TT, Volovik GE. High-temperature surface superconductivity in topological flat-band systems. Phys Rev B 2011;83:220503.
[36] Philip TV, Beck PA. CsCl-type ordered structures in binary alloys of transition elements. JOM 1957;9:1269–71.
[37] Laves F, Wallbaum HJ. Crystal Chemistry of Titanium Alloys. Naturwissenschaften 1939;27:674.
[38] Eremenko VN, Shtepa TD, Sirotenko VG. Intermediate phases in alloys of titanium with iridium, rhodium, and osmium. Powder Metall Met Ceram 1966;5:487–90.
[39] Hafner J. Materials simulations using VASP—A quantum perspective to materials science. Comput Phys Commun 2007;177:6–13.
[40] Reshak AH. Spin-polarized second harmonic generation from the antiferromagnetic CaCoSO single crystal. Sci Rep 2017;7:46415.
[41] Reshak AH. Ab initio study of TaON, an active photocatalyst under visible light irradiation. Phys Chem Chem Phys 2014;16:10558–65.
[42] Davydyuk GE, Khyzhun OY, Reshak AH, Kamarudin H, Myronchuk GL, Ganylchuk SP, et al. Photoelectrical properties and the electronic structure of $Tl_{1-x}In_{1-x}Sn_xSe_2$ (x = 0, 0.1, 0.2, 0.25) single crystalline alloys. Phys Chem Chem Phys 2013;15:6965–72.
[43] Reshak AH, Kogut YM, Fedorchuk AO, Zamuruyeva OV, Myronchuk GL, Parasyuk OV, et al. non-linear optical susceptibilities and the hyperpolarizability of the mixed crystals $Ag_{0.}$ $5P_{b1.75}Ge(_{S1-x}Se_x)_4$: Experiment and theory. Phys Chem Chem Phys 2013;15:18979.
[44] Reshak AH, Stys D, Auluck S, Kityk IV. Dispersion of linear and nonlinear optical susceptibilities and the hyperpolarizability of 3-methyl-4-phenyl-5-(2-pyridyl)-1, 2, 4-triazole. Phys Chem Chem Phys 2011;13:2945–52.
[45] Reshak AH. $Fe_2MnSi_xGe_{1-x}$: influence thermoelectric properties of varying the germanium content. RSC Adv 2014;4:39565.
[46] Reshak AH. Thermoelectric properties for AA-and AB-stacking of a carbon nitride polymorph (C_3N_4). RSC Adv 2014;4:63137.
[47] Perdew JP, Burke K, Ernzerhof M. Perdew, Burke, and Ernzerhof reply. Phys Rev Lett 1998;80.
[48] Perdew JP, Burke K, Ernzerhof M. Generalized gradient approximation made simple. Phys Rev Lett 1996;77:3865.
[49] Wu QS, Zhang SN, Song HF, Troyer M, Soluyanov AA. WannierTools: An open-source software package for novel topological materials. Computer Phys Commun 2018:224405–16.
[50] Marzari N, Vanderbilt D. Maximally localized generalized Wannier functions for composite energy bands. Phys Rev B 1997;56:12847.
[51] Souza I, Marzari N, Vanderbilt D. Maximally localized Wannier functions for entangled energy bands. Phys Rev B 2001;65:035109.
[52] Taylor J, Guo H, Wang J. Ab initio modeling of quantum transport properties of molecular electronic devices. Phys Rev B 2001;63:245407.
[53] Du Y, Tang F, Wang D, Sheng L, Kan EJ, Duan CG, et al. CaTe: a new topological node-line and Dirac semimetal. npj Quant Mater 2017;2:3.
[54] Heyd J, Scuseria GE. Efficient hybrid density functional calculations in solids: Assessment of the Heyd-Scuseria-Ernzerhof screened Coulomb hybrid functional. J Chem Phys 2004;121:1187–92.
[55] Zhang J, Li X, Yang J. Electrical control of carriers' spin orientation in the FeVTiSi Heusler alloy. J Mater Chem C 2015;3:2563–7.
[56] He J, Ding G, Zhong C, Li S, Li D, Zhang G. Cr_2TiC_2-based double MXenes: Novel 2D bipolar antiferromagnetic semiconductor with gate-controllable spin orientation toward antiferromagnetic spintronics. Nanoscale 2019;11:356.
[57] Thelander C, Björk MT, Larsson MW, Hansen AE, Wallenberg LR, Samuelson L. Electron transport in InAs nanowires and heterostructure nanowire devices. Solid State Commun 2004;131:573.
[58] Yamakage A, Yamakawa Y, Tanaka Y, Okamoto Y. Line-Node Dirac Semimetal and Topological Insulating Phase in Noncentrosymmetric Pnictides CaAgX (X = P, As). J Phys Soc Japan 2015;85(1):013708.